J Biomol NMR (2011) 50:103–117
DOI 10.1007/s10858-011-9505-5

ARTICLE

Solution structure, dynamics and thermodynamics of the three SH3 domains of CD2AP

Jose L. Ortega Roldan · Martin Blackledge · Nico A. J. van Nuland · Ana I. Azuaga

Received: 18 November 2010 / Accepted: 24 February 2011 / Published online: 26 April 2011

Abstract CD2 associated protein (CD2AP) is an adaptor protein that plays an important role in cell to cell union needed for the kidney function. It contains three N-terminal SH3 domains that are able to interact among others with CD2, ALIX, c-Cbl and Ubiquitin. To understand the role of the individual SH3 domains of this adaptor protein we have performed a complete structural, thermodynamic and dynamic characterization of the separate domains using NMR and DSC. The energetic contributions to the stability and the backbone dynamics have been related to the structural features of each domain using the structure-based FoldX algorithm. We have found that the N-terminal SH3 domain of both adaptor proteins CD2AP and CIN85 are the most stable SH3 domains that have been studied until now. This high stability is driven by a more extensive network of intra-molecular interactions. We believe that this increased stabilization of N-terminal SH3 domains in adaptor proteins is crucial to maintain the necessary conformation to establish the proper interactions critical for the recruitment of their natural targets.

Keywords Adaptor protein · CD2AP · NMR · Protein structure · SH3 domain

Abbreviations

CD2AP	CD2 associated protein
DLS	Dynamic light scattering
NMR	Nuclear magnetic resonance
NOESY	Nuclear overhauser enhancement spectroscopy
RDC	Residual dipolar coupling
RMSD	Root mean square deviation
SH3	Src-homology domain 3
DSC	Differential scanning calorimetry
TOCSY	Total correlation spectroscopy

Introduction

SH3 domains are probably the most common molecular recognition modules in the proteome (Mayer 2001; Li 2005). All SH3 domains share the same three-dimensional structure that consists of two orthogonal sheets of three anti-parallel beta-strands. A considerable amount of work has been carried out to characterize these domains in terms of their stability, folding thermodynamics and kinetics, three-dimensional structure, backbone and side chain dynamics and interactions with artificial ligands and natural targets (Filimonov et al. 1999; Guijarro et al. 1998; Plaxco et al. 1998; Viguera et al. 1994). Kinetic and equilibrium studies indicate that the folding-unfolding of these domains is a simple two-state process, without significantly populated intermediates. More recent results

J. L. O. Roldan · A. I. Azuaga
Departamento de Química Física e Instituto de Biotecnología, Facultad de Ciencias, Universidad de Granada, Fuentenueva s/n, 18071 Granada, Spain

M. Blackledge
Protein Dynamics and Flexibility by NMR, Institut de Biologie Structurale Jean-Pierre Ebel, CEA, CNRS, UJF UMR 5075, 41 Rue Jules Horowitz, Grenoble 38027, France

N. A. J. van Nuland (✉)
Structural Biology Brussels, Vrije Universiteit Brussel, Pleinlaan 2, 1050 Brussels, Belgium
e-mail: nvnuland@vub.ac.be

N. A. J. van Nuland
Department of Molecular and Cellular Interactions, VIB, Pleinlaan 2, 1050 Brussels, Belgium

suggest that the SH3 domain shows an elevated, but not full structural cooperativity and therefore the conformational fluctuations of the different structural elements are partially coupled (Casares et al. 2007). Such structural cooperativity implies that any local energetic change or interaction gets transmitted efficiently to the rest of the structure.

The majority of these studies have focussed on single SH3 containing proteins. In many proteins, however, SH3 domains occur in tandems of two or three units separated by short or long stretches of linking residues. Some of these proteins, such as those of the CIN85/CMS (Cbl-Interacting protein of 85 kDa/Cas ligand with Multiple SH3 domains) adaptor protein family, show high homology among their SH3 domains suggesting similar specificities in ligand binding (Dikic 2002). It has been reported previously that different domains are able to transmit information along a protein via conformational changes (Bendsen et al. 2009; Calvete 2004) or the modification of internal dynamics (Lenaerts et al. 2008).

CD2 associated protein (CD2AP) is an adaptor protein that belongs to the CIN85/CMS adaptor proteins family. CD2AP knockout mice exhibit nephrotic syndrome characterized by defects in podocyte foot processes, suggesting that CD2AP plays an essential role in cell-to-cell union needed for the kidney function (Shih et al. 1999; Li et al. 2000). CD2AP is a cytosolic protein of 641 amino acids. The amino terminus consists of three SH3 domains (SH3 A, B and C) and a proline rich region, which is followed by a globular domain and a coiled-coil structure.

As a first step toward understanding the role of the three CD2AP SH3 domains, we have carried out a complete structural, dynamic and thermodynamic characterization of the isolated domains. The thermal stability of each individual domain has been studied by Differential Scanning Calorimetry (DSC), allowing a systematic comparison between the stabilities of the different SH3 domains. The three dimensional solution structure of each individual domain was determined under identical experimental conditions, permitting a structure-based explanation for the differences in stability found between the different SH3 domains. Moreover, the contribution of each residue to the global folding was studied by NMR Hydrogen Deuterium (H/D) exchange, and its relationship with backbone dynamics was evaluated with the information extracted from ^{15}N relaxation experiments.

Our results on the CD2AP SH3 domains reveal significant differences in the global folding parameters and the backbone dynamics of the three domains, as well as differences compared to diverse SH3 domains found in the literature and predictions based on the structures of SH3 domains of the homologous adaptor protein CIN85. These differences are explained in terms of individual energetic contributions arising from their sequence and three-dimensional structures, and rationalized in term of their biological role in the context of the adaptor proteins.

Materials and methods

Protein expression and purification

Unlabelled CD2AP SH3-A was obtained as described (Moncalian et al. 2006). ^{15}N-labeled and ^{13}C, ^{15}N-labeled CD2AP SH3-A and SH3-C were obtained as described (Ortega Roldan et al. 2007). CD2AP SH3-B and SH3-C gene, originally cloned in the plasmid pGEX 4T1 with BamH-I and Xho-I, were sub-cloned in a pGAT-2 plasmid with Nco-I and Hind-III covalently linked to a N-terminal 6xHis tag, a GST tag and a Thrombin cleavage site. Unlabelled SH3-B and C were produced by growing on TB medium at 27°C till an OD_{600} of 0.7. Protein expression was induced with 1 mM IPTG at 27°C and cells were grown overnight. Both proteins were purified as described in (Ortega Roldan et al. 2007). Sample concentration was determined spectrophotometrically using extinction coefficients of 9,970, 12,490 and 14,980 M^{-1} cm^{-1} for SH3-A, B and C, respectively, determined using the ProtParam tool (Expasy).

Differential scanning calorimetry and dynamic light scattering

Temperature scans were performed as described in (Varela et al. 2009) at a concentration of 1 mg/mL in a VP-DSC microcalorimeter (Microcal, Northampton, MA, USA). Unfolding experiments were carried out in 20 mM Glycine, 20 mM Sodium Acetate or 20 mM Sodium Phosphate buffers at different pH values from 2.0 to 7.4 Calorimetric data was analysed as described in (Varela et al. 2009). Dynamic light scattering (DLS) measurements were carried out on a DynaPro MS-X instrument (Wyatt Technology Corporation, Santa Barbara, CA, USA) as described in (Varela et al. 2009). Unfolding and DLS experiments were carried out in 20 mM Glycine, 20 mM Sodium Acetate or 20 mM Sodium Phosphate buffers at different pH values from 2.0 to 7.4.

NMR spectroscopy

Assignment

^{15}N-labeled and ^{13}C, ^{15}N-labeled samples of CD2AP SH3-A and C and unlabelled samples of SH3-B were prepared for NMR experiments at 1 mM in 92% H_2O/8% D_2O, 50 mM NaPi pH 6.0. 1 mM DTT was added to SH3-B and C samples. NMR spectra were recorded on a Varian NMR

Direct-Drive Systems 600 MHz spectrometer (^{1}H frequency of 600.25 MHz). Assignment of SH3-A and C domains was carried out as previously described (Ortega Roldan et al. 2007). Due to the high tendency to aggregate of SH3-B (less than 2 days), we used the homonuclear assignment method (Wuthrich 1986) by recording two-dimensional NOESY and TOCSY spectra on an unlabelled sample of SH3-B with mixing times of 125 and 70 ms, respectively. Water was suppressed using the excitation sculpting method (Hwang and Shaka 1998). All NMR data were processed using NMRPipe (Delaglio et al. 1995) and analyzed by NMRView (Johnson 2004) or Sparky (Goddard and Kneller 1993).

Measurement of residual dipolar couplings

Residual dipolar couplings (RDCs) were measured in samples partially aligned in a liquid-crystalline medium consisting of a mixture of 5% penta-ethyleneglycol monododecyl ether ($C^{12}E^5$) and hexanol (Ruckert and Otting 2000). $^1D_{NH}$ RDCs were measured in the SH3-A domain from a pair of spin-state-selected ^{1}H-^{15}N correlation spectra recorded using an DIPSAP filter (Brutscher 2001) for J-mismatch compensated spin-state selection, and the BEST concept for longitudinal relaxation and sensitivity enhancement (Lescop et al. 2007; Schanda et al. 2006) on a Varian NMR Direct-Drive Systems 600 MHz spectrometer. $^1D_{NH}$, $^1D_{C\alpha C}$, $^2D_{HNC'}$ and $^1D_{C\alpha H\alpha}$ RDCs were measured in the SH3-C domain as described (Ortega-Roldan et al. 2009).

RDC refinement of the SH3-A and C domains of CD2AP

The refinement of the structures of SH3-A was carried out using the program SCULPTOR (Hus et al. 2000), which runs under CNS (Brunger et al. 1998). The protocol involves a restrained MD calculation using the standard CNS force field. The solution structure of SH3-A was obtained by refining two different initial X-ray structures of the domain determined in the absence and presence of CD2 peptide (PDB 2J6 K and 2J6O, respectively) (Moncalian et al. 2006). The backbone conformation is initially restricted to its X-ray coordinates using a harmonic potential and a distance restraint file calculated from all H_α-HN distances lower than 10 Å in the SH3-A free X-ray structure and refined using $^1D_{NH}$ RDCs. The SH3-C structure was obtained from the refinement of the SH3-C pH 2.0 NMR structure (PDB entry 2JTE) using $^1D_{NH}$, $^1D_{C\alpha C'}$, $^2D_{HN\ C'}$ and $^1D_{C\alpha H\alpha}$ RDCs measured in a PEG/n-hexanol mixture with the program SCULPTOR (Hus et al. 2000). The backbone conformation was restricted in this calculation using the NOe restraints obtained at pH 2.0. The five lowest-energy structures of each set of refined SH3-A domain and the ten lowest-energy structures of SH3-C domain were used for the final analysis.

Structure calculation of the SH3-B domain of CD2AP

All ^{1}H except for labile side-chain protons were assigned from 600 MHz 2D TOCSY and NOESY spectra. NOe cross peaks were obtained by automatic peak picking in the 2D NOESY followed by manual removal of diagonal peaks and peaks arising from artefacts (e.g. residual water). NOes were assigned using the automated NOe assignment procedure of CYANA version 2.1 (Guntert et al. 1997; Herrmann et al. 2002). The standard protocol was used with seven cycles of combined automated NOe assignment and structure calculation of 100 conformers in each cycle. Unambiguously assigned restraints were used for a final structure refinement in explicit solvent using the RECOORD protocol, which runs under CNS (Nederveen et al. 2005). The ten lowest-energy structures were used for final analysis.

Amide hydrogen deuterium exchange

Seventy microliters of concentrated samples (3,5 mM) of CD2AP ^{15}N labeled SH3-A and C were dissolved in 500 μL of ^2H_2O at pH 6.0. ^{15}N 2D SOFAST-HMQCs (Schanda et al. 2005; Schanda and Brutscher 2006) were acquired at 25°C at different times until a decay of approximately 90% of the slowest exchanging proton for SH3-A and C respectively. Spectra of 1024*32 complex points were recorded using a relaxation delay of 500 ms resulting in a total experimental time of 5' 36'' and 5' 47'' for SH3-A and C. Hydrogen exchange rates and the Gibbs free energy ΔG_{ex} per residue were calculated as described in (Casares et al. 2007).

Backbone dynamics from ^{15}N relaxation data

The relaxation parameters ^{15}N R_1, R_2, and ^{1}H-^{15}N steady-state NOe were measured at 600.25 MHz and 25°C of CD2AP SH3-A and C. Relaxation values were obtained from series of 2D experiments with coherence selection achieved by pulse field gradients using the experiments described previously (Farrow et al. 1994) on ^{15}N-labelled SH3-A and C. The ^{1}H-^{15}N heteronuclear NOes were determined from the ratio of peak intensities (I_{on}/I_{off}) with and without the saturation of the amide protons for 3 s. ^{15}N R_1 and ^{15}N R_2 relaxation rates were measured from spectra with different relaxation delays: 10, 100, 200, 300, 400, 500, 700, 900, 1200 and 1500 ms for R_1 and 10, 30, 50, 70, 90, 110, 150, 190 and 250 ms for R_2. Relaxation parameters and their corresponding errors were extracted with the program NMRView. Reduced spectral density mapping

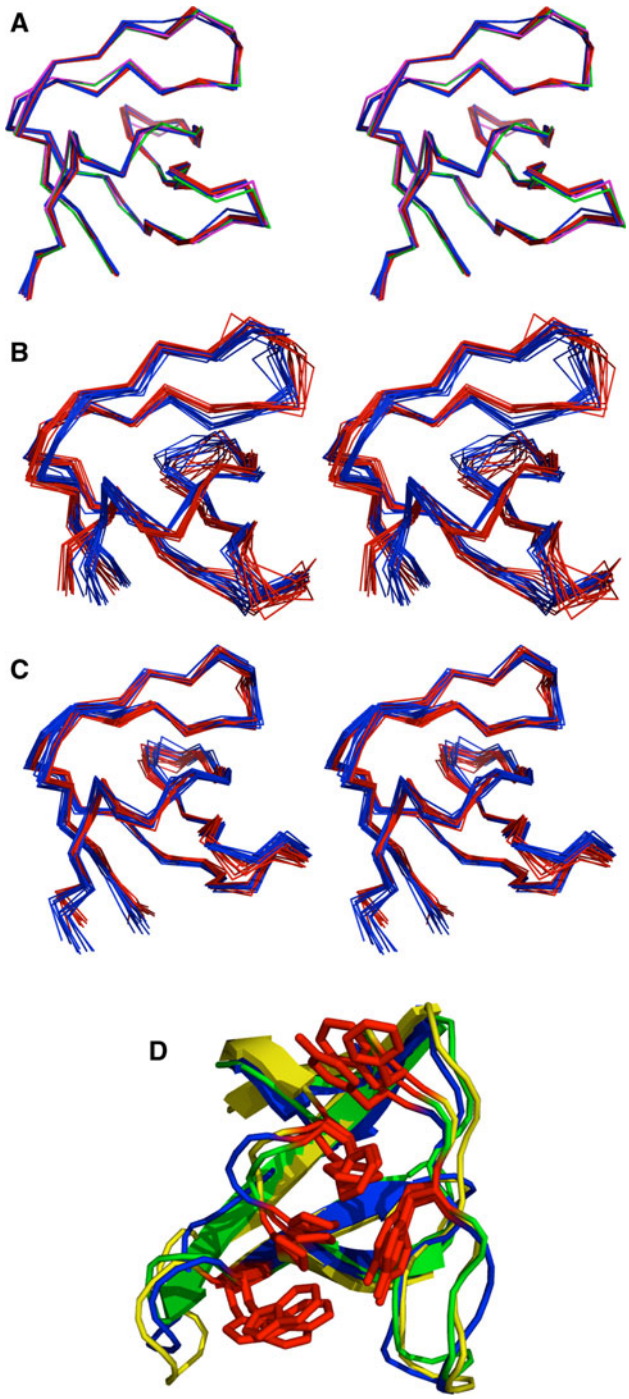

Fig. 1 **a** Stereo ribbon representation of the ensemble of the ten lowest energy solution structures of CD2AP SH3-A. Structures resulting from 2J6K refinement are coloured *blue*, structures from 2J6O refinement red. For comparison, the X-ray structures of CMS SH3-A in the free (PDB entry 2J6K) and CD2-bound form (PDB entry 2J6O) are shown in *green* and *magenta*, respectively. Structures were superimposed on the backbone atoms of residues 3-58. **b** Stereo ribbon representation of the ensemble of the ten lowest energy structures of CD2AP SH3-B (*blue*) and CMS SH3-B (PDB entry 2FEI, *red*) superimposed on the backbone atoms of residues 6-60 (3-57 in CMS SH3-B). **c** Stereo ribbon representation of the ensemble of the ten lowest energy structures of CD2AP SH3-C at pH 2 (*red*) and the RDC-refined at pH 6 (*blue*) superimposed on the backbone atoms of residues 6-64 **d** Cartoon representation of the lowest energy structure of CD2AP SH3-A (*blue*), SH3-B (*green*) and SH3-C (*yellow*). The residues involved in polyproline binding are presented in *red* sticks

was applied following published procedures (Markus et al. 1996).

Results

The solution structures of the three SH3 domains of CD2AP

In order to rationalize the stabilities of each of the three SH3 domains of CD2AP in terms of their structure, we have determined the high-resolution solution structures of each individual domain under the same experimental conditions at pH 6.0. All backbone resonances of SH3-A and C were assigned from 3D HNCACB, CBCA(CO)NH, HNCO and HBHA(CO)NH experiments (BMRB accession numbers 16643 and 16641, respectively). All proton resonances of SH3-B, except for the labile side-chain hydrogen atoms, were assigned from homonuclear 2D TOCSY and 2D NOESY ^{1}H NMR spectra (BMRB accession number 16642).

SH3-A

Imposing 56 NH RDCs measured in a PEG/n-hexanol mixture on the two crystal structures resolved at 2.3 and 2.0 Å resolution respectively, lead to the same unique structure (Deposited in the Protein Data Bank with accession number 2KRM) (Fig. 1a) that shows satisfactory agreement with the experimental RDCs as observed in Fig. 2b; the backbone RMSD for residues 3-56 between the lowest-energy structure of each set is 0.32 Å, the same as the variation within each structural set (RMSD of 0.25 Å and 0.32 Å, respectively; see Table 1), confirming the effectiveness of the protocol used. Figure 2a shows that the calculated RDCs from the respective X-ray structures differ from the experimental determined RDCs in a similar manner.

SH3-B

The solution structure of the SH3-B domain was obtained using unambiguously assigned NOes from the automatic NOe assignment protocol in CYANA (Guntert 1997; Guntert et al. 1997) in a subsequent water-refinement with RECOORD (Nederveen et al. 2005) (Deposited in the Protein Data Bank with accession number 2KRN). Even though the structure is obtained from only distance

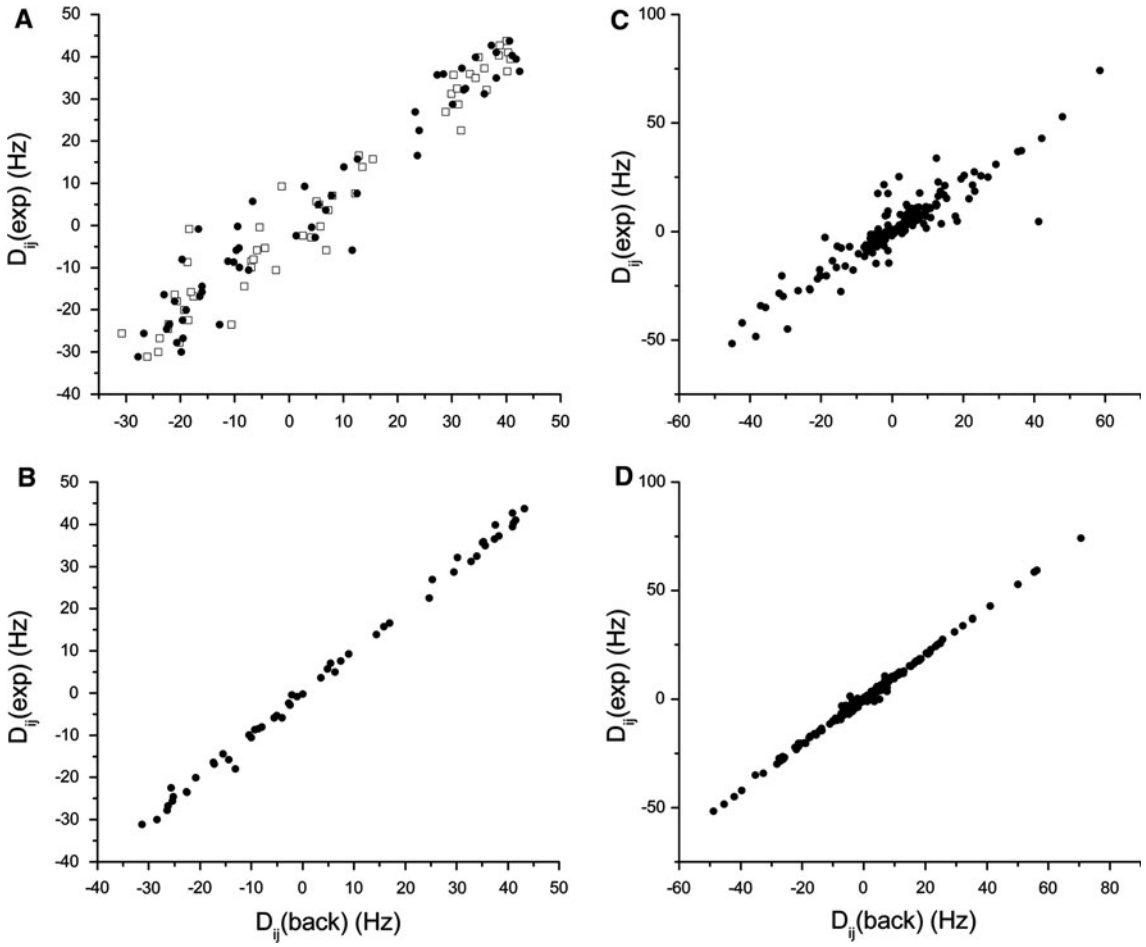

Fig. 2 Experimental versus back-calculated RDCs plots. **a** Experimental $^{1}D_{NH}$ RDCs measured versus back-calculated RDCs from PDB 2J6O (*circles*) and 2J6 K (*open squares*). **b** Experimental $^{1}D_{NH}$ RDCs measured versus back-calculated RDCs from the lowest energy RDC-refined SH3-A structure. **c** Experimental $^{1}D_{NH}$, $^{1}D_{C\alpha C'}$, $^{2}D_{HN\ C'}$ and $^{1}D_{C\alpha H\alpha}$ RDCs measured for SH3-C versus back-calculated RDCs from the NMR structure of SH3-C at pH 2 (PDB 2JTE). **d** Experimental $^{1}D_{NH}$, $^{1}D_{C\alpha C'}$, $^{2}D_{HN\ C'}$ and $^{1}D_{C\alpha H\alpha}$ RDCs measured for SH3-C versus back-calculated RDCs from the lowest energy RDC-refined SH3-C structure

restraints derived from homonuclear NOe spectra, the ensemble shows very good Ramachandran statistics while fulfilling the experimental data (Table 1), reflecting the high quality of the 3D structures. The average backbone RMSD for residues 6-58 is 0.77 ± 0.10 Å, which is similar to the 0.75 ± 0.14 Å found for the same residues in the ensemble of 10 lowest-energy NMR structures of the highly homologous SH3-B from the human equivalent CMS (PDB entry 2FEI; see Fig. 1b), which was obtained from heteronuclear NMR data. Moreover, these two SH3-B structures are similar with a backbone RMSD of 1.09 Å for the same residues between the lowest-energy structures of the two NMR ensembles.

SH3-C

The SH3-C structure was obtained from the refinement of the SH3-C pH 2.0 NMR structure (PDB entry 2JTE) using $^{1}D_{NH}$, $^{1}D_{C\alpha C'}$, $^{2}D_{HN\ C'}$ and $^{1}D_{C\alpha H\alpha}$ RDCs measured in a PEG/n-hexanol mixture with the program SCULPTOR (Hus et al. 2000) (Deposited in the Protein Data Bank with accession number 2KRO). The ensemble fulfils the experimental data (Table 1, Fig. 1c) with excellent Ramachandran statistics, reflecting the high quality of the 3D structures. A significant improvement in the correlation of the back-calculated and the experimental RDCs is clearly observed in Fig. 2c and d. The average backbone RMSD for residues 8-62 is 0.61 ± 0.10 Å, which is slightly higher than the 0.49 ± 0.09 Å found for the same residues in the ensemble of 10 lowest-energy NMR structures determined at pH 2 from only NOes (PDB entry 2JTE; see Fig. 1c). The higher RMSD found for the RDC refined structure at pH 6.0 is caused by the increased backbone dynamics present in the RT and n-Src loop and the C-terminus at this pH compared to pH 2.0 (Ortega Roldan et al. 2007). The structural differences between the two sets are small with a

Table 1 Structural statistics for the 10 lowest energy structures of CD2AP SH3 A, B and C domains

	SH3-A	SH3-B	SH3-C
Distance restraints			
Short range (i–j = 0)	–	225	237
Medium range (1 ≤ |i–j| ≤ 4)	–	304	403
Long range (|ii–j| ≥ 5)	–	312	394
Orientation restraints			
Residual dipolar couplings	56	0	227
Restraint statistics			
NOE violations > 0.5 Å	–	0	0
RDC violations > 3 Hz	1	–	1
RDC violations > 5 Hz	0	–	0
RMSD from average (Å)	Residues 3–56	Residues 6–58	Residues 8–62
Backbone N, CA, C′	0.28 ± 0.06	0.77 ± 0.10	0.61 ± 0.10
Heavy atoms	1.62 ± 0.14	1.48 ± 0.10	1.29 ± 0.16
Ramachandran plot			
Most favored regions (%)	86.5	84.9	86.5
Additional allowed regions (%)	13.5	13.1	11.5
Generously allowed regions (%)	0.0	1.2	0.0
Disallowed regions (%)	0.0	0.8	1.9

Flexible N- and C-terminal residues were omitted from the RMSD analysis. NOe violations and Ramachandran statistics obtained from PROCHECK-NMR analysis over all residues

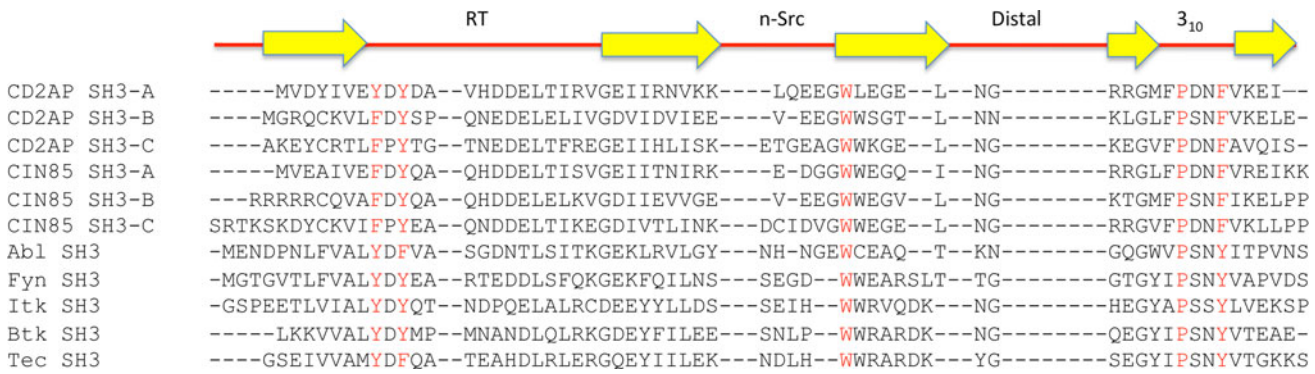

Fig. 3 Sequence alignment of the CD2AP SH3 domains with other related and non-related SH3 domains. Residues involved in binding to proline-rich sequences are shown in *red*

backbone RMSD of 0.94 Å for the same residues between the lowest-energy structures of the two NMR ensembles.

Comparison between the three SH3 domains of CD2AP

The three SH3 domains of CD2AP studied here are highly homologous (Fig. 3). Sequence alignment shows highest similarity between the SH3-A and C domains, with 53.2% of identity, followed by a 51% identity between SH3-B and C and a 46.2% identity between SH3-A and B. They share the typical aromatic residues involved in binding to proline rich sequences, but differ in the length of the n-Src loop where SH3-C has one or two additional residues compared to the A and B domain, respectively. The CD2AP SH3 domains do not only show high sequence identity among themselves, but sequence alignment with other SH3 domains (Fig. 3) reveals high homology with the SH3 domains of the adaptor protein CIN85, suggesting targeting of similar natural partners (Dikic 2002).

The three CD2AP SH3 domains show the five β-strands and the 3^{10} helix that are common in the family of SH3 domains (Fig. 1d). They also contain all the features that are typically found in other SH3 domains, including the canonical binding site residues for the recognition of polyproline sequences that consist of a hydrophobic surface with three shallow pockets defined by the side chains of

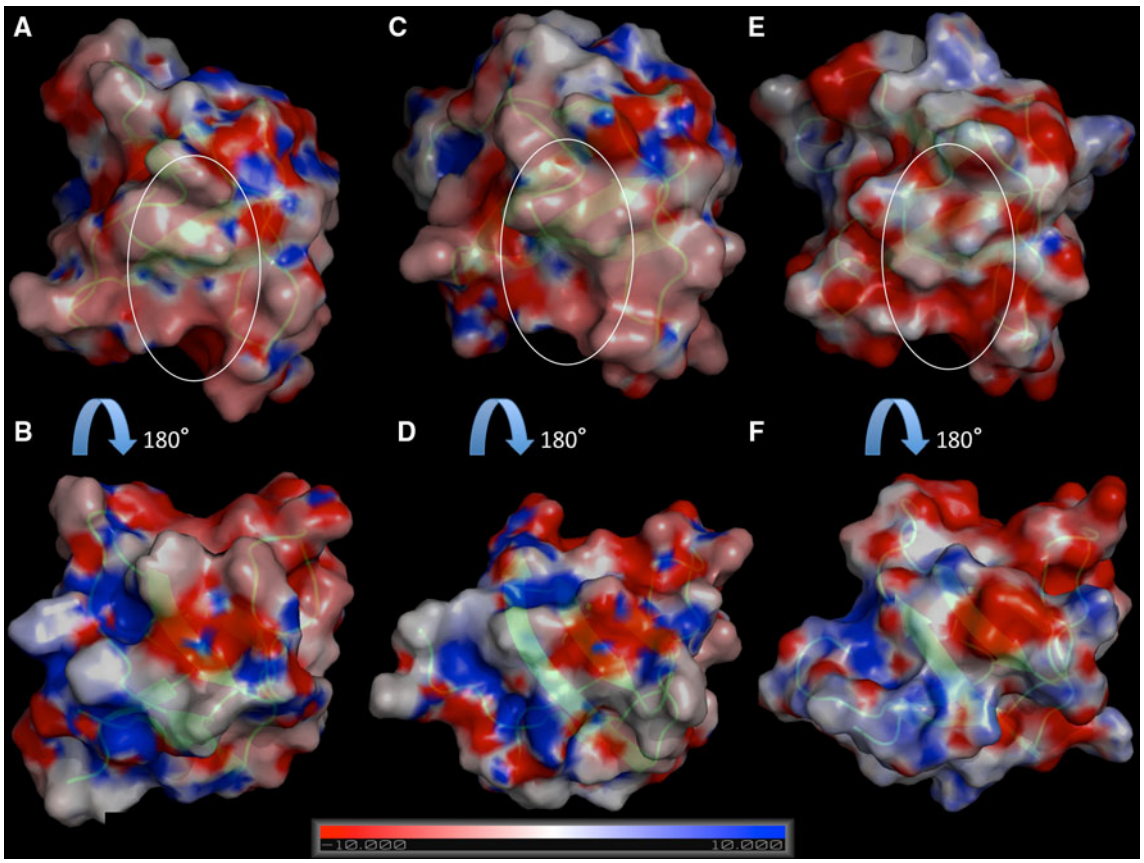

Fig. 4 Surface representation in 180° rotated orientations of CD2AP SH3-A (**a** and **b**), SH3-B (**c** and **d**) and SH3-C (**e** and **f**) domains, showing the surface-charge distribution. The electrostatic surface representation of the three structures was drawn using Pymol (www.pymol.org) using a Poisson-Boltzman electrostatics calculation (Dolinsky et al. 2004). Orientations in **a**, **c** and **e** are similar than in Fig. 1d. The polyproline binding pocket is indicated by a *circle* in each domain

preserved aromatic residues that are indicated in Figs. 1d and 3. The high sequence similarity is reflected in substantial structural homology, with backbone RMSD of 1.36 Å and 1.20 Å for residues 3-32 and 37-56 in SH3-A and residues 6-35 and 39-58 in SH3-B compared to the equivalent residues 8-37 and 43-62 in SH3-C, and 1.29 Å between SH3-A and SH3-B for the same residues. The flexible N and C-termini, as well as the n-Src loop were excluded in this analysis, the latter due to its different length in the three CD2AP SH3 domains.

Figure 4 shows the surface-charge distribution of the three SH3 domains. A large polar surface area is found in each domain. SH3-A and SH3-B share a very similar electrostatic distribution with positive and negative charges distributed similarly over the whole structural surface. In the polyproline binding area (highlighted with a white circle) a mainly non-polar surface is found in SH3-A and SH3-B, flanked by positively and negatively charged residues. In contrast SH3-C displays a different electrostatic distribution in this area, presenting a highly negatively charged surface. The rest of the domain shows a similar charge distribution as in the other two domains.

Table 2 Pairs of amino-acids involved in salt bridges in CD2AP SH3-A, B and C

SH3-A	SH3-B	SH3-C
D3–R27	E18–K47	E7–K36
E7–K55	E22–K47	E27–R10
D9–R21	E58–R5	E47–H32
D16–H14		E52–K45
D16–R45		
E17–H14		
E29–R21		
E39–R46		
E41–R27		
E41–R46		
D51–K31		
E56–K58		

In order to relate the structural features of the three domains with their thermodynamic behaviour, the optimal hydrogen bonding network and salt bridges were calculated for each structure using the Whatif WEB interface (Hooft et al. 1996). Table 2 shows the pairs of amino-acids

Table 3 Thermodynamic data obtained from DSC experiments for CD2AP SH3 domains at different pH values

pH	T_m (°C)	ΔH (kJ/mol)	ΔG (25°C) (kJ/mol)	ΔC_p^a (kJ/mol molK)
SH3-A				
2.0	42.2 ± 0.8	168 ± 3	7.7 ± 0.5	3.5 ± 0.1
3.0	55.4 ± 0.8	211 ± 3	14.5 ± 0.6	
6.0	68.1 ± 0.8	256 ± 3	22.4 ± 0.8	
7.0	66.5 ± 0.8	253 ± 3	21.7 ± 0.7	
SH3-B				
5.5	53.7 ± 0.9	176 ± 4	12 ± 2.2	2.3 ± 0.2
6.5	53.2 ± 1	154 ± 10[b]		
7.0	53.4 ± 1	194 ± 10[b]		
7.4	51.8 ± 1	207 ± 10[b]		
SH3-C				
2.0	47.2 ± 0.9	190 ± 4	11.7 ± 0.7	1.9 ± 0.2
2.5	48.6 ± 0.9	194 ± 4	12.6 ± 0.7	
3.0	52.5 ± 0.9	204 ± 4	15,0 ± 0.8	
3.5	57.0 ± 0.9	208 ± 4	17,1 ± 0.8	
4.0	58.7 ± 0.9	213 ± 4	18,3 ± 0.9	
6.0	54.6 ± 0.9	220 ± 10[c]	16.0 ± 1.3	
7.0	50.4 ± 0.9	173 ± 10[c]	13.6 ± 1.1	

[a] ΔC_p of unfolding calculated from the slope of ΔH versus T_m. All other ΔH values were obtained from a two-state unfolding model

[b] ΔH estimated by integrating the area under the unfolding thermal transition

[c] ΔH estimated from the plot of ΔH versus T_m

involved in salt bridges. In particular SH3-A exploits a high number of salt bridges, which is the result of the uniform distribution of positively and negatively charged residues over the whole structure as visualized in Fig. 4. At the same time a different number of hydrogen bonds are found in the three domains, varying from 35 in SH3-A, 39 in SH3-B and 33 in SH3-C. The stabilization of the C-terminus of SH3-C is particularly remarkable due to hydrogen bonding and salt bridge network via the β-sheet formed by the β_1, β_2 and β_5 strands. Such a network is absent in SH3-A, while direct interactions between the C- and N- terminus are present in SH3-B.

Thermal stability studied by DSC

The global stability of the three SH3 domains of CD2AP was measured by DSC at different pH values in order to explore, in combination with the NMR-detected H/D exchange, the nature of the native state conformational ensemble of the three domains. Prior to the DSC experiments the association state of every sample was analyzed with Dynamic Light Scattering (DLS) at 25°C. A hydrodynamic radius of 1.6 nm was obtained for all CD2AP SH3 domains, a value typical for a globular monomeric protein of this size (Wilkins et al. 1999; Varela et al. 2009; Morel et al. 2006). For the SH3-B domain, however, a small fraction of higher-order associated states was found.

SH3-A

DSC experiments of the CD2AP SH3-A domain were carried out at pH values 2.0, 3.0, 6.0, and 7.0. For the pH range between 2.0 and 3.0 and between 6.0 and 7.0 the unfolding thermal transitions are consistent with a two-state criteria (Viguera et al. 1994). Table 3 summarizes the thermodynamic data at all pH values studied. Both the enthalpy and Gibbs energy of unfolding reach a maximum at pH 6.

SH3-B

DSC experiments were performed at pH 5.5, 6.5 and 7.4. Due to massive aggregation in the dialysis tube, no calorimetric study was possible in the pH range 2.0 to 4.0. Only at pH 5.5 the unfolding thermal transitions were partially reversible and show a unique transition with a T_m centred at 53.7°C. The reheating experiment shows two transitions, one centred at the same T_m as the one observed in the first scan, corresponding to the unfolding of the monomeric domain, and a high temperature second transition centred at 85°C. The latter transition can be explained as the unfolding of high molecular species observed by DLS (data not shown). No concentration or scan rate effect is present on the first transition of the sample, and the molar heat capacity curves accounted very well by the two-state unfolding model. At pH 6.0 and 7.4 the unfolding thermal transitions were completely irreversible. In this case, no reversible thermodynamic model can be applied and the calorimetric ΔH was estimated by integrating the area under the unfolding thermal transition and T_m was determined from its maximum.

SH3-C

DSC experiments were carried out at pH 2.0, 2.5, 3.0, 4.0, 6.0 and 7.0. In the pH range between 2.0 and 4.0 all unfolding thermal transitions were mostly reversible and independent of concentration and scan rate, although the reversibility is pH dependent, and decreases upon increasing the pH to values close to the theoretical isoelectric point (pI 4.6). However, the reversibility in this pH range is always higher than 80%. For these conditions the molar heat capacity curves were fitted using a two-state unfolding model (Fig. 5a). All calorimetric data are summarized in Table 3. An increase in stability is found when raising the pH from 2.0 to 4.0. At pH values higher than 4 the thermal unfolding is partially reversible. At pH 6.0, thermal transitions halted a few degrees after the T_m were

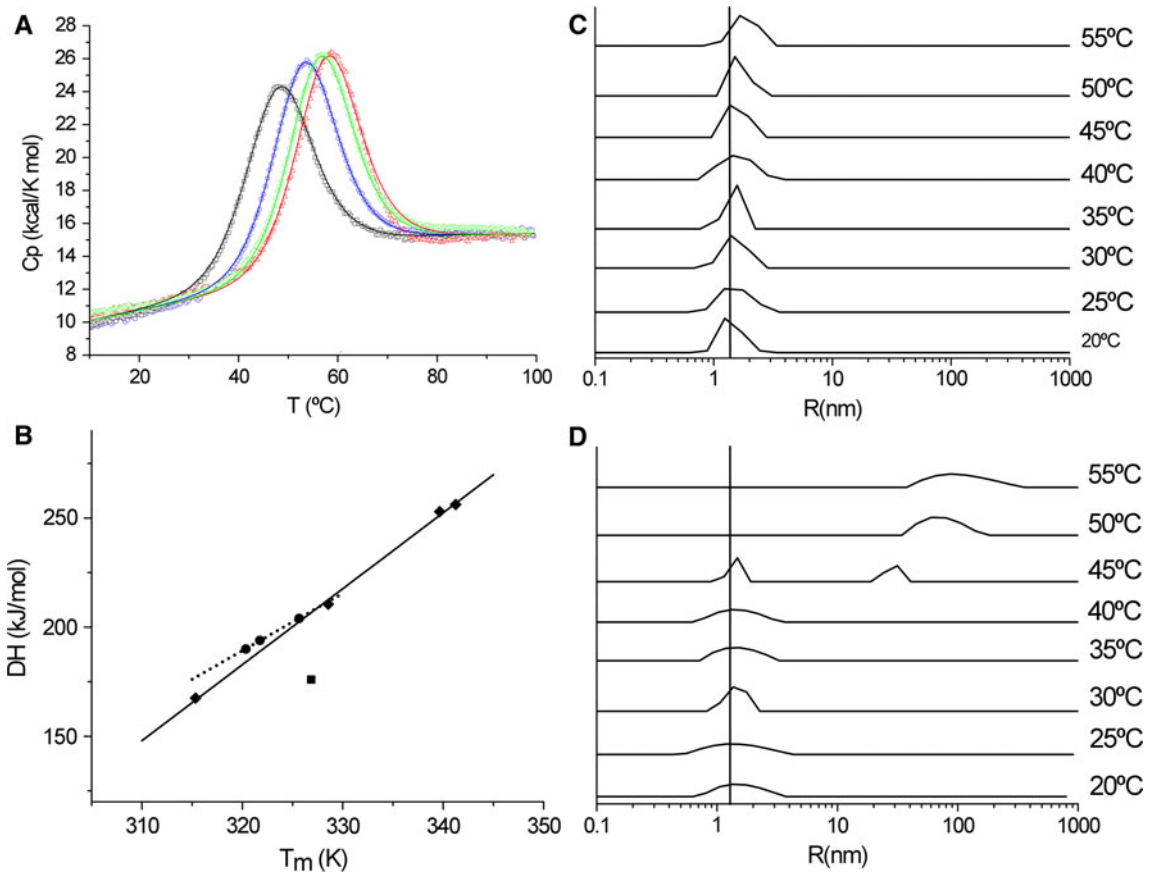

Fig. 5 **a** DSC thermograms of CD2AP SH3-C at pH 2.0 (*black*), 3.0 (*blue*), 3.5 (*green*) and 4.0 (*red*). *Solid lines* show best fits using a two-state unfolding model. **b** ΔH versus T_m plot and linear fittings for SH3-A (*filled diamond* and *solid line*), SH3-C (*filled circle* and *dotted line*) and ΔH versus T_m at pH 5.5 for SH3-B (*filled square*). **c** Size distribution obtained by DLS at different temperatures for SH3-C at pH 2.0. *Vertical line* centred at a hydrodynamic radius of 1.6 nm. **d** Size distribution obtained by DLS at different temperatures for SH3-C at pH 4.0. *Vertical line* centred at a hydrodynamic radius of 1.6 nm

highly reversible and the T_m is not affected by the irreversible process that appears at higher temperature. Therefore, the enthalpy can be estimated from the T_m of this transition using the plot of ΔH vs T_m (Fig. 5b). DLS experiments were performed at different temperatures to check the presence of associated states at high and low temperatures. At pH 2.0 no aggregates are present at any temperature (Fig. 5c), consistent with the high reversibility of the thermal unfolding transition measured by DSC. The shift of the peak centred at 1.6 nm when raising the temperature to 2.1 nm is typical for denaturation of globular monomers into an unfolded polypeptide chain of this size (Wilkins et al. 1999; Morel et al. 2006). At pH 4.0 the thermal unfolding followed by DLS shows the appearance of states with higher hydrodynamic radius when raising the temperature above 45°C, consistent with the decrease in reversibility found at this pH observed by DSC (Fig. 5d).

Comparison of the thermodynamic properties of the three domains indicates a different behaviour of SH3-B compared with SH3-A and C caused by its higher tendency to aggregate. At pH values below the pI SH3-A and C show unfolding thermal transitions that can be fitted to a two-state unfolding model and present a similar increase in stability and decrease in reversibility upon increasing the pH. At pH values above the pI, a small decrease in stability is found in SH3-C, with ΔG values of 16.0 and 13.6 kJ/mol at pH 6.0 and 7.0, coupled with a lost of reversibility in the thermal unfolding, while SH3-A shows a reversible thermal unfolding and much higher stability reflected in ΔG values of 22.4 and 21.7 kJ/mol at pH 6.0 and 7.0 (Table 3).

Conformational flexibility and backbone dynamics from hydrogen/deuterium (H/D) exchange and ^{15}N relaxation data

H/D experiments were performed in order to relate the global unfolding parameters obtained from DSC with the structural features of CD2AP SH3-A and C domains. No data could be extracted for SH3-B due to aggregation during the preparation of the sample.

H/D exchange rates have been measured at pH 6.0 for SH3-A and C. Reliable data could be extracted for 37

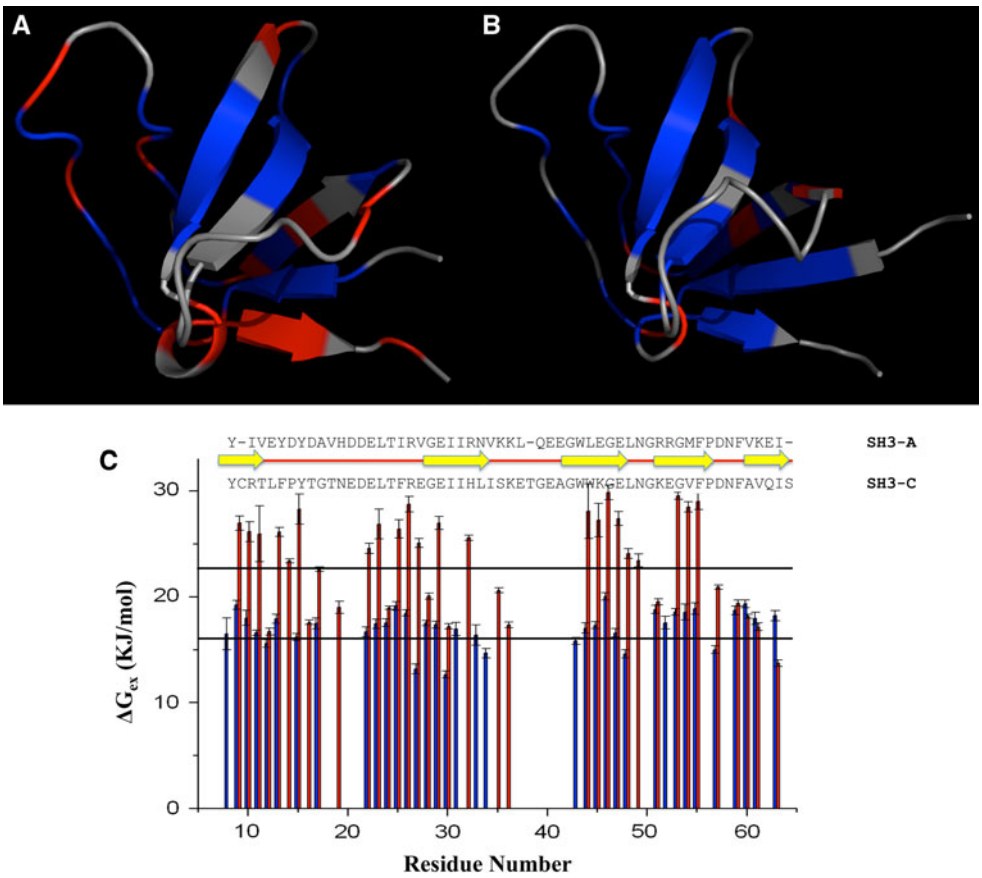

Fig. 6 Plot of the cooperative core and the flexible regions undergoing partial unfolding on the structures of CD2AP SH3-A (**a**) and SH3-C (**b**). Residues with ΔG_{ex} higher than the ΔG obtained by DSC minus three standard deviations (3std) are represented in *blue*. Residues with $\Delta G_{ex} < \Delta G$-3std are represented in *red*. Residues exchanging within the dead time of the experiment are represented in *grey*. **c** ΔG_{ex} calculated from H/D exchange for SH3-A (*red*) and SH3-C (*blue*), superimposed on the SH3-C sequence. *Black lines* indicate the ΔG obtained by DSC for SH3-A and C domains (*Upper* and *lower line*, respectively)

residues out of 62 in SH3-A and 38 out of 64 residues in SH3-C. In all cases the exchange shows first-order kinetics and allows an accurate determination of the exchange rate constants, k_{ex}, assuming an EX2 mechanism. The experimental ΔG_{ex} per residue are shown in Fig. 6c. In both SH3 domains, protected residues are grouped mainly in six regions of the protein sequence, corresponding to different elements of secondary structure.

In the case of SH3-A, the RT and distal loop show measurable protection, including histidine 14, located at the edge of the RT loop. In contrast, the n-Src loop does not show measurable protection. One non-observable proline residue is present in position 50. Comparison of the protection pattern between the different secondary structure elements shows high and similar ΔG_{ex} values except for the C-terminal region (residues 51-57), including the 3^{10} helix and the fifth β-sheet. The core of the protein is therefore constituted by the β_1, β_3 and β_4 strands and the two arms of the RT loop, as they present individual ΔG_{ex} of the same order as the ΔG obtained by DSC. On the other hand, lower ΔG_{ex} values are found in β_2 and β_5 strands and the 3^{10} helix indicating a higher flexibility of these areas (Fig. 6a).

In the case of the SH3-C domain, similarly to SH3-A, the n-Src loop does not show measurable protection. In contrast, RT and distal loops show much lower protection to exchange in SH3-C. For this domain, all secondary structure elements show comparable ΔG_{ex} values which are similar to the ΔG obtained by DSC and thus form the cooperative core of the protein (Fig. 6b).

^{15}N relaxation measurements give information on the ps to ns and μs to ms timescale of the backbone dynamics, complementing the ms to second timescale dynamics provided by the H/D exchange. The molecular rotational correlation time τ_c was calculated for SH3-A and SH3-C using the program TENSOR2 (Dosset et al. 2000) from selected R_2/R_1 values of residues that are not affected by extensive disorder on a ps time scale (low NOe) or chemical exchange on a μs-ms time scale (elevated R_2/R_1 ratio), corresponding to residues 4-10, 26, 28-30, 44-49, 55-56 in SH3-A and residues 9-12, 28-33, 45-47, 52, 56, 60-62 in SH3-C. Molecular rotational correlation times of 4.24 and 3.55 ns were obtained for SH3-A and C respectively, corresponding to a radius of hydration of 17.1 Å and 16.1 Å, values expected for globular monomeric molecules of this size (Wilkins et al. 1999; Morel et al. 2006; Varela et al. 2009). Moreover, these values are in good agreement with the hydrodynamic radius obtained with DLS at much lower concentrations, indicating no association phenomena in this range of concentrations. The relaxation data are

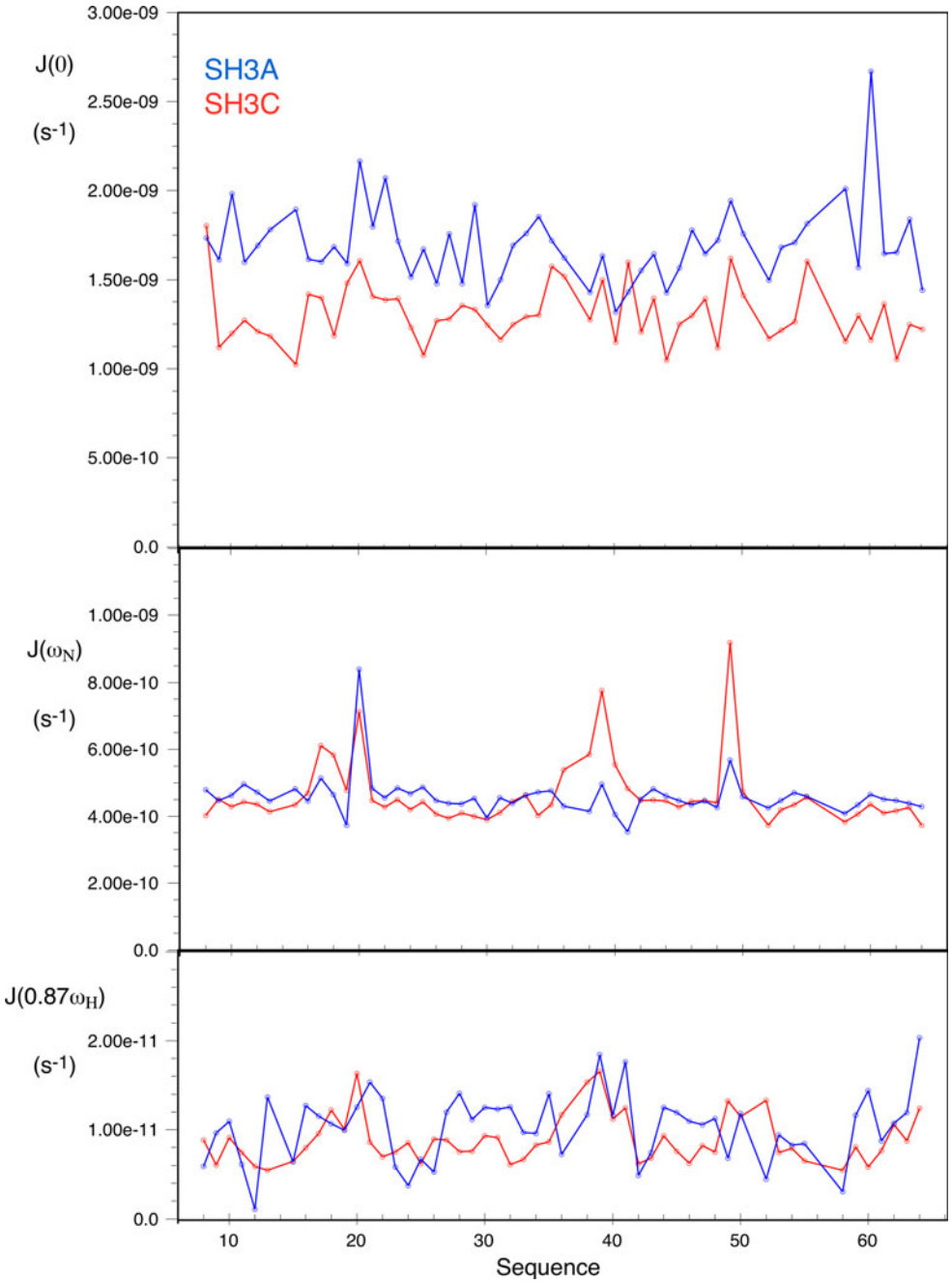

Fig. 7 Backbone dynamics of CD2AP SH3-A (*blue*) and SH3-C (*red*) measured at 600.25 MHz and 25°C, expressed in terms of reduced spectral density mapping (*top* J(0), *middle* J(ω_N) *bottom* J(0.87ω_H)

shown in the form of reduced spectral density mapping for both domains in Fig. 7. High-frequency motions, on the ps-sub nanosecond timescale are similar for both domains (J(ω_H)), while pronounced increases in J(0) and to a lesser extent J(ω_N), are indicative of an increase in low frequency motions for SH3A. Average R_2 values for SH3-A and SH3-C are 7.0 ± 0.8 s^{-1} and 5.6 ± 0.6 s^{-1} in the secondary structural elements, while average R_1 values are 2.4 ± 0.1 s^{-1} and 2.3 ± 0.1 s^{-1}. We prefer to present the data in this format, rather than using a standard Lipari-Szabo type model-free analysis, because of the difficulty of separating contributions from overall rotational diffusion and internal motion when significant nanosecond motions appear to be present. This kind of problem is particularly acute for small molecules, where the overall rotational correlation coefficient is less then 5 ns.

Discussion and conclusions

SH3 domains are small modular domains involved in protein–protein interactions. The sequence identity

between different SH3 domains is low, ranging from 15 to 45% (Larson and Davidson 2000), although all SH3 domains adopt a similar five-stranded β-barrel structure. In the present work, we have determined the three dimensional solution structures of the three SH3 domains of CD2AP at pH 6.0. A high sequence homology is found between the domains, and with other related adaptor proteins, such as CIN85, what is translated into a high structural homology (Figs. 1d and 3). Moreover, the aromatic residues that are involved in recognition of polyproline sequences (Fig. 1d) are similarly positioned in the three CD2AP SH3 domains. A similar electrostatic distribution is found on the surface around the polyproline binding pocket in SH3-A and B, dominated by a large negative area in the specificity pocket and a non-polar surface in the hydrophobic pockets surrounded by positively and negatively charged residues, consistent with the overlapping specificities suggested elsewhere (Dikic 2002). However, SH3-C presents a higher negatively charged surface around the hydrophobic pockets. Interestingly, differences are found between CIN85 SH3-C and CD2AP SH3-C in this area. CIN85 SH3-C displays a more positively charged region around the hydrophobic pockets, similar to the A and B domains of both CIN85 and CD2AP, indicating possible differences in binding affinities and specificity to natural targets.

Despite of the similarity between the three dimensional structures of the CD2AP SH3 domains, except for the n-Src loop orientation, differences are found in the number and distribution of intra-molecular interactions. A computational structure based energy calculation using the program FoldX (Guerois et al. 2002) has been carried out in order to relate the contribution of the interactions to the stability with the experimental thermodynamic parameters obtained by DSC. The contribution of these intra-molecular interactions to the unfolding ΔG is reflected in the enthalpy change of unfolding (ΔH). This value is dominated by two terms: a positive contribution due to the disruption of internal interactions (hydrogen bonds, van der Waals, salt bridges, etc.) and a negative term resulting from the solvation of groups that are buried in the native state (Sadqi et al. 1999). FoldX predicts a higher enthalpy value for SH3-A domain driven by a 1 kJ/residue higher hydrogen bond energy than SH3-C and a 0.7 to 1.57 kJ/res higher van der Waals energy than SH3-B and C as no significant differences are found in this term due to the solvation of polar and hydrophobic groups. Nevertheless, similar hydrogen bond energy contribution to the ΔH is found in SH3-B. This result is consistent with the higher number of hydrogen bonds predicted by Whatif for SH3-A and B. On the other hand, the experimental enthalpy values obtained for SH3-B are lower than the predicted ones, probably due to inaccuracy in the experimental value caused by the presence of high molecular weight species even at room temperature and neutral pH that were observed in the DLS experiments. As no major differences are found in the entropy term calculated from thermodynamic data for the three CD2AP SH3 domains, the 0.2 kJ/res higher stability of SH3-A at 25°C is assumed to be driven by the enthalpic term.

The global unfolding data obtained by DSC has been compared with local unfolding information obtained by NMR detected amide H/D exchange in SH3-A and C domains. No information could be extracted for SH3-B due to its high tendency to aggregate. The stable cores of both SH3 domains, defined as those regions where individual ΔG_{ex} are of the same order than the ΔG obtained by DSC, comprise most of the secondary structural elements, except for the C-terminal part of SH3-A where lower ΔG_{ex} values are found. The amide exchange of these core residues thus occurs primarily via a global unfolding reaction, while in the β_5 strand and the C-terminus in SH3-A, H/D exchange takes place via local or subglobal unfolding processes. This indicates a higher flexibility of this region of the protein. This effect is also appreciable on a different timescale from the higher J(0) contribution derived from ^{15}N relaxation values of residues in this region, indicating that this area is affected by low frequency motions. The increased mobility in the C-terminus of the SH3-A domain allows a higher flexibility in the junction with the rest of CD2AP that may permit regulation of interactions of the SH3-B or C domains or other regions of the protein with natural targets.

The higher number of hydrogen bonds and salt-bridges present in SH3-A compared to SH3-C not only results in a higher stability at 25°C but also affects the backbone flexibility via the different distribution of the intra-molecular interactions along the sequence. Lower amplitude contributions to $J(\omega_N)$ are found for the RT, n-Src and Distal loops in SH3-A, consistent with a higher number of hydrogen bonds and salt-bridges calculated in these regions from the structure. This extended hydrogen bonding network is confirmed by H/D exchange data, where measurable protection is found for His 14 in the RT loop, Val 29 and Lys 30 in the n-Src loop, and Gly 44 in the Distal loop of SH3-A. The lower flexibility exhibited in these loops in SH3-A is in contrast to that observed in SH3-C and other SH3 domains, where increased flexibility is generally found for RT, n-Src and Distal loops (Ferreon et al. 2003; Wang et al. 2001; Horita et al. 2000). Thus the lower flexibility of the backbone of CD2AP SH3-A domain is related with the higher overall stability resulting from the more extended intramolecular interaction network along the structure. Furthermore, comparison of R_2/R_1 values for SH3-C measured at pH 2.0 and 6.0 reveals similar motions for SH3-C at low pH as SH3-A at pH 6.0, in agreement with the similar thermal stability observed at low pH values for SH3-A and C. These results suggest that the backbone

flexibility of the SH3 domains closely correlates with the overall thermal stability as observed for other systems (Jarymowycz and Stone 2006).

The stability of the CD2AP SH3 domains has been compared with the thermal stability of other non-related SH3 domains of Abl, Fyn, Itk, Btk and Tec (Filimonov et al. 1999; Knapp et al. 1998). While CD2AP SH3-B and C show experimental ΔG values from DSC in the same order than the compared SH3 domains, SH3-A shows an average 0.20 kJ/res higher experimental stability. No major differences in charge distributions are observed between the CD2AP SH3 domains and the Fyn, Abl, Itk, Btk and Tec SH3 domains, indicating that differences in thermal stability do not arise from differences in the electrostatic distribution in the surface of the domains. CD2AP SH3-A displays up to 1.5 kJ/res higher experimental ΔH than Fyn, Abl, Itk, Btk and Tec SH3 domains. In order to explain these enthalpy differences, each individual contribution to ΔH have been calculated from the structure using the program FoldX. For all non-related SH3 domains an average 1.07 kJ/res lower hydrogen bond energy term is found, providing a possible explanation for the experimental ΔH differences. Differences in the experimental values of ΔC_p are also found. CD2AP SH3 domains display up to 0.8 kJ/K mol lower values than the mean ΔC_p found in literature for SH3 domains. ΔC_p differences arise from the different changes in average polar and non-polar surface accessibilities between the folded and the extended unfolded state. The difference in total, non-polar and polar surface accessibility is bigger in the Fyn, Abl, Itk, Tec and Btk SH3 domains than in the CD2AP SH3 domains, resulting in lower predicted ΔC_p values for the CD2AP SH3 domains, thus in agreement with the experimental results (Luque and Freire 1998). The higher thermal stability shown by the CD2AP SH3-A compared to non-related SH3 domains can be explained then by a higher ΔH caused by a more extensive intramolecular interaction network as observed by H/D exchange and ^{15}N relaxation measurements.

No experimental thermodynamic data can been found in literature for adaptor proteins containing multiple SH3 domains in tandem. In order to compare the thermodynamic data obtained for CD2AP with other adaptor proteins with similar domain structure, the SH3 domains of the related CIN85 were analyzed using FoldX. We used the structures of the three CIN85 SH3 domains determined by either NMR or X-ray (PDB entries 2BZ8, 2O6O and 2K9G for SH3-A, B and C, respectively). CIN85 shows a very high sequence homology with CD2AP, ranging from 68.4% of homology for both N-terminal SH3 domains to 67.3% of homology between central SH3 domains and 58.2% of homology between the C-terminal SH3 domains (see Fig. 3). In both proteins, the N-terminal SH3 domain displays very similar hydrogen bonding, van der Waals and solvation energies, suggesting closely similar enthalpy values. Moreover, similar enthalpy values are predicted for the second and third SH3 domains despite the differences in energy contributions, with higher hydrogen bond energies but lower solvation energies. This analysis suggests that such an elevated stability for an N-terminal SH3 domain might be a general characteristic of multiple domain containing proteins. As stated previously, the CD2AP SH3-A domain displays an average 0.20 kJ/res higher experimental ΔG than Abl, Fyn, Brk, Itk and Tec SH3 domains at physiological pH values. All these domains are located in the middle of the sequence of their full-length proteins, and in some cases, like Abl SH3 domain, the presence of a N-terminal domain is required to maintain its three dimensional structure (Chen et al. 2008). The high ΔG observed in CD2AP SH3-A and predicted for CIN85 SH3-A suggest that N-terminal SH3 domains need a very high stability in order to maintain a correctly folded conformation to establish the proper interactions crucial for the recruitment of their natural targets. On the other hand, SH3-B and C show similar ΔG values per residue to the other RTK SH3 domains, indicating that SH3 domains located away from the N-terminus do not need such stabilization. Indeed, binding studies performed in our group confirm that all three SH3 domains bind to CD2, but with a significant higher affinity to the N-terminal domain (unpublished data).

We have shown the relationship between sequence, three dimensional structure, stability, and dynamics of single SH3 domains and rationalized it in terms of their function inside the adaptor proteins. The work presented here will form the basis for a better understanding on how interactions of each individual domain to their natural targets are affected by the presence of the others. Work on different CD2AP SH3 domain tandems is in progress in our group to address this question.

Acknowledgments This research was funded by grant BIO2005-04650 from the Spanish Ministry of Education and Science (MEC) and FQM-02838 from the Andalucia Regional Goverment. We thank Manuel Iglesias-Bexiga and Maria-Luisa Romero-Romero for initial experimental work, Malene Ringkjobing-Jensen for help with the RDC measurement, Salvador Casares and Francisco Conejero-Lara for useful discussions and Obdulio Lopez-Mayorga for his continuous support. J.L.O.R. is supported by a pos-doctoral grant from the University of Granada. The CD2AP SH3-A clone was kindly provided by Jeronimo Bravo. The 600 MHz spectra were recorded in the Centre for Scientific Instrumentation (CIC) of the University of Granada and at the RALF Large Scale Facility in Grenoble, which is funded by the 'Access to Research Infrastructures' program of the European Union. The CD2AP SH3-B structure calculation was carried out in the supercomputing facilities (UGRGrid) of the University of Granada.

References

Bendsen S, Oestergaard VH, Skouboe C, Brinch M, Knudsen BR, Andersen AH (2009) The QTK loop is essential for the communication between the N-terminal ATPase domain and the central cleavage–ligation region in human topoisomerase IIalpha. Biochemistry 48(27):6508–6515. doi:10.1021/bi900 5978

Brunger AT, Adams PD, Clore GM, DeLano WL, Gros P, Grosse-Kunstleve RW, Jiang JS, Kuszewski J, Nilges M, Pannu NS, Read RJ, Rice LM, Simonson T, Warren GL (1998) Crystallography & NMR system: a new software suite for macromolecular structure determination. Acta Crystallogr D Biol Crystallogr 54(Pt 5):905–921

Brutscher B (2001) Accurate measurement of small spin-spin couplings in partially aligned molecules using a novel J-mismatch compensated spin-state-selection filter. J Magn Reson 151(2):332–338. doi:10.1006/jmre.2001.2375

Calvete JJ (2004) Structures of integrin domains and concerted conformational changes in the bidirectional signaling mechanism of alphaIIbbeta3. Exp Biol Med (Maywood) 229(8):732–744. doi:229/8/732[pii]

Casares S, Lopez-Mayorga O, Vega MC, Camara-Artigas A, Conejero-Lara F (2007) Cooperative propagation of local stability changes from low-stability and high-stability regions in a SH3 domain. Proteins 67(3):531–547. doi:10.1002/prot.21284

Chen S, Dumitrescu TP, Smithgall TE, Engen JR (2008) Abl N-terminal cap stabilization of SH3 domain dynamics. Biochemistry 47(21):5795–5803. doi:10.1021/bi800446b

Delaglio F, Grzesiek S, Vuister GW, Zhu G, Pfeifer J, Bax A (1995) NMRPipe: a multidimensional spectral processing system based on UNIX pipes. J Biomol NMR 6(3):277–293

Dikic I (2002) CIN85/CMS family of adaptor molecules. FEBS Lett 529(1):110–115. doi:S0014579302031885[pii]

Dolinsky TJ, Nielsen JE, McCammon JA, Baker NA (2004) PDB2PQR: an automated pipeline for the setup of Poisson-Boltzmann electrostatics calculations. Nucleic acids research 32 (Web Server issue):W665–W667. doi:10.1093/nar/gkh381

Dosset P, Hus JC, Blackledge M, Marion D (2000) Efficient analysis of macromolecular rotational diffusion from heteronuclear relaxation data. J Biomol NMR 16(1):23–28

Farrow NA, Muhandiram R, Singer AU, Pascal SM, Kay CM, Gish G, Shoelson SE, Pawson T, Forman-Kay JD, Kay LE (1994) Backbone dynamics of a free and phosphopeptide-complexed Src homology 2 domain studied by 15 N NMR relaxation. Biochemistry 33(19):5984–6003

Ferreon JC, Volk DE, Luxon BA, Gorenstein DG, Hilser VJ (2003) Solution structure, dynamics, and thermodynamics of the native state ensemble of the Sem-5 C-terminal SH3 domain. Biochemistry 42(19):5582–5591. doi:10.1021/bi030005j

Filimonov VV, Azuaga AI, Viguera AR, Serrano L, Mateo PL (1999) A thermodynamic analysis of a family of small globular proteins: SH3 domains. Biophys Chem 77(2–3):195–208

Goddard TD, Kneller DG (1993) Sparky 3, University of California, San Francisco

Guerois R, Nielsen JE, Serrano L (2002) Predicting changes in the stability of proteins and protein complexes: a study of more than 1000 mutations. J Mol Biol 320(2):369–387. doi:10.1016/S0022-2836(02)00442-4

Guijarro JI, Morton CJ, Plaxco KW, Campbell ID, Dobson CM (1998) Folding kinetics of the SH3 domain of PI3 kinase by real-time NMR combined with optical spectroscopy. J Mol Biol 276(3):657–667. doi:10.1006/jmbi.1997.1553

Guntert P (1997) Calculating protein structures from NMR data. Methods Mol Biol 60:157–194. doi:10.1385/0-89603-309-0:157

Guntert P, Mumenthaler C, Wuthrich K (1997) Torsion angle dynamics for NMR structure calculation with the new program DYANA. J Mol Biol 273(1):283–298. doi:10.1006/jmbi.1997.1284

Herrmann T, Guntert P, Wuthrich K (2002) Protein NMR structure determination with automated NOE-identification in the NOESY spectra using the new software ATNOS. J Biomol NMR 24(3):171–189. doi:5111821[pii]

Hooft RW, Sander C, Vriend G (1996) Positioning hydrogen atoms by optimizing hydrogen-bond networks in protein structures. Proteins 26(4):363–376. doi:10.1002/(SICI)1097-0134(199612)26:4<363:AID-PROT1>3.0.CO;2-D

Horita DA, Zhang W, Smithgall TE, Gmeiner WH, Byrd RA (2000) Dynamics of the Hck-SH3 domain: comparison of experiment with multiple molecular dynamics simulations. Protein Sci 9(1):95–103. doi:10.1110/ps.9.1.95

Hus JC, Marion D, Blackledge M (2000) De novo determination of protein structure by NMR using orientational and long-range order restraints. J Mol Biol 298(5):927–936. doi:10.1006/jmbi.2000.3714

Hwang TL, Shaka AJ (1998) Multiple-pulse mixing sequences that selectively enhance chemical exchange or cross-relaxation peaks in high-resolution NMR spectra. J Magn Reson 135(2):280–287. doi:10.1006/jmre.1998.1598

Jarymowycz VA, Stone MJ (2006) Fast time scale dynamics of protein backbones: NMR relaxation methods, applications, and functional consequences. Chem Rev 106(5):1624–1671. doi:10.1021/cr040421p

Johnson BA (2004) Using NMRView to visualize and analyze the NMR spectra of macromolecules. Methods Mol Biol 278:313–352. doi:10.1385/1-59259-809-9:313

Knapp S, Mattson PT, Christova P, Berndt KD, Karshikoff A, Vihinen M, Smith CI, Ladenstein R (1998) Thermal unfolding of small proteins with SH3 domain folding pattern. Proteins 31(3):309–319. doi:10.1002/(SICI)1097-0134(19980515)31:3<309:AID-PROT7>3.0.CO;2-D[pii]

Larson SM, Davidson AR (2000) The identification of conserved interactions within the SH3 domain by alignment of sequences and structures. Protein Sci 9(11):2170–2180. doi:10.1110/ps.9.11.2170

Lenaerts T, Ferkinghoff-Borg J, Stricher F, Serrano L, Schymkowitz JW, Rousseau F (2008) Quantifying information transfer by protein domains: analysis of the Fyn SH2 domain structure. BMC Struct Biol 8:43. doi:10.1186/1472-6807-8-43

Lescop E, Schanda P, Brutscher B (2007) A set of BEST triple-resonance experiments for time-optimized protein resonance assignment. J Magn Reson 187(1):163–169. doi:10.1016/j.jmr.2007.04.002

Li SS (2005) Specificity and versatility of SH3 and other proline-recognition domains: structural basis and implications for cellular signal transduction. Biochem J 390(Pt 3):641–653. doi:10.1042/BJ20050411

Li C, Ruotsalainen V, Tryggvason K, Shaw AS, Miner JH (2000) CD2AP is expressed with nephrin in developing podocytes and is found widely in mature kidney and elsewhere. Am J Physiol Renal Physiol 279(4):F785–F792

Luque I, Freire E (1998) Structure-based prediction of binding affinities and molecular design of peptide ligands. Methods Enzymol 295:100–127

Markus MA, Dayie KT, Matsudaira P, Wagner G (1996) Local mobility within villin 14T probed via heteronuclear relaxation measurements and a reduced spectral density mapping. Biochemistry 35(6):1722–1732. doi:10.1021/bi951933o

Mayer BJ (2001) SH3 domains: complexity in moderation. J Cell Sci 114(Pt 7):1253–1263

Moncalian G, Cardenes N, Deribe YL, Spinola-Amilibia M, Dikic I, Bravo J (2006) Atypical polyproline recognition by the CMS N-terminal Src homology 3 domain. J Biol Chem 281(50): 38845–38853. doi:10.1074/jbc.M606411200

Morel B, Casares S, Conejero-Lara F (2006) A single mutation induces amyloid aggregation in the alpha-spectrin SH3 domain: analysis of the early stages of fibril formation. J Mol Biol 356(2):453–468. doi:10.1016/j.jmb.2005.11.062

Nederveen AJ, Doreleijers JF, Vranken W, Miller Z, Spronk CA, Nabuurs SB, Guntert P, Livny M, Markley JL, Nilges M, Ulrich EL, Kaptein R, Bonvin AM (2005) RECOORD: a recalculated coordinate database of 500 + proteins from the PDB using restraints from the BioMagResBank. Proteins 59(4):662–672. doi: 10.1002/prot.20408

Ortega Roldan JL, Romero Romero ML, Ora A, Ab E, Lopez Mayorga O, Azuaga AI, van Nuland NA (2007) The high resolution NMR structure of the third SH3 domain of CD2AP. J Biomol NMR 39(4):331–336

Ortega-Roldan JL, Jensen MR, Brutscher B, Azuaga AI, Blackledge M, van Nuland NA (2009) Accurate characterization of weak macromolecular interactions by titration of NMR residual dipolar couplings: application to the CD2AP SH3-C:ubiquitin complex. Nucleic Acids Res 37(9):e70

Plaxco KW, Guijarro JI, Morton CJ, Pitkeathly M, Campbell ID, Dobson CM (1998) The folding kinetics and thermodynamics of the Fyn-SH3 domain. Biochemistry 37(8):2529–2537. doi: 10.1021/bi972075u

Ruckert M, Otting G (2000) Alignment of Biological Macromolecules in Novel Nonionic Liquid Crystalline Media for NMR Experiments. J Am Chem Soc 122(32):7793–7797. doi:10.1021/ja001068h

Sadqi M, Casares S, Abril MA, Lopez-Mayorga O, Conejero-Lara F, Freire E (1999) The native state conformational ensemble of the SH3 domain from alpha-spectrin. Biochemistry 38(28): 8899–8906. doi:10.1021/bi990413g

Schanda P, Brutscher B (2006) Hadamard frequency-encoded SOFAST-HMQC for ultrafast two-dimensional protein NMR. J Magn Reson 178(2):334–339. doi:10.1016/j.jmr.2005.10.007

Schanda P, Kupce E, Brutscher B (2005) SOFAST-HMQC experiments for recording two-dimensional heteronuclear correlation spectra of proteins within a few seconds. J Biomol NMR 33(4): 199–211. doi:10.1007/s10858-005-4425-x

Schanda P, Van Melckebeke H, Brutscher B (2006) Speeding up three-dimensional protein NMR experiments to a few minutes. J Am Chem Soc 128(28):9042–9043. doi:10.1021/ja062025p

Shih NY, Li J, Karpitskii V, Nguyen A, Dustin ML, Kanagawa O, Miner JH, Shaw AS (1999) Congenital nephrotic syndrome in mice lacking CD2-associated protein. Science 286(5438):312–315. doi:7865[pii]

Varela L, Morel B, Azuaga AI, Conejero-Lara F (2009) A single mutation in an SH3 domain increases amyloid aggregation by accelerating nucleation, but not by destabilizing thermodynamically the native state. FEBS Lett 583(4):801–806. doi:10.1016/j.febslet.2009.01.033

Viguera AR, Martinez JC, Filimonov VV, Mateo PL, Serrano L (1994) Thermodynamic and kinetic analysis of the SH3 domain of spectrin shows a two-state folding transition. Biochemistry 33(8):2142–2150

Wang C, Pawley NH, Nicholson LK (2001) The role of backbone motions in ligand binding to the c-Src SH3 domain. J Mol Biol 313(4):873–887. doi:10.1006/jmbi.2001.5083

Wilkins DK, Grimshaw SB, Receveur V, Dobson CM, Jones JA, Smith LJ (1999) Hydrodynamic radii of native and denatured proteins measured by pulse field gradient NMR techniques. Biochemistry 38(50):16424–16431. doi:bi991765q[pii]

Wuthrich K (1986) NMR of proteins and nucleic acids